Pharmazie

Pharmazie **2026**; 81(11): 56395
https://doi.org/10.31083/Pharmazie56395

Research Article

Conjugation of Nosiheptide to a Bidentate Catechol to Overcome Permeability Limitations in a Gram-Negative Model Strain

Shixin Zheng[1], Jing Li[2], Jingchao Ji[3], Chang Liu[2,*]

[1]Medical School, Shandong Xiehe University, 250109 Jinan, Shandong, China
[2]School of Chemistry and Chemical Engineering, University of Jinan, 250022 Jinan, Shandong, China
[3]Department of Pharmacy, Shandong Provincial Third Hospital, Shandong University, 250031 Jinan, Shandong, China
*Correspondence: 597511639@qq.com (Chang Liu)
Academic Editors: Michał Tomczyk and Walter E. Müller
Submitted: 27 July 2026 Revised: 14 October 2026 Accepted: 29 October 2026 Published: 19 November 2026

Abstract

Background: Antibiotic penetration to intracellular targets is severely restricted by the outer membrane barrier of Gram-negative bacteria. Nosiheptide (NOS, **16**) is potent against Gram-positive bacteria but ineffective against the tested Gram-negative model strain because its large molecular size limits efficient membrane penetration. Siderophore conjugation provides a "Trojan horse" strategy that exploits bacterial iron uptake pathways to overcome this permeability barrier. **Methods:** Bidentate catechol siderophore mimetics (**15a–15d**) were synthesized and used to construct a siderophore–NOS conjugate (**17**). The antibacterial activity of conjugate **17** was evaluated against *Pseudomonas aeruginosa* PAO1. The role of siderophore-mediated uptake was investigated by comparing antibacterial activity under iron-depleted and iron-rich conditions, alongside a transporter-deficient mutant strain. Molecular docking was performed to compare the interactions of conjugate **17** and nosiheptide with the ribosomal target, and confocal fluorescence imaging of *Escherichia coli* was conducted to assess cellular uptake. **Results:** Conjugate **17** exhibited antibacterial activity against *P. aeruginosa* PAO1, particularly under iron-limited conditions. The reduced antibacterial activity under iron-rich conditions suggests that bacterial pathways involved in iron acquisition may contribute to the uptake of conjugate **17**. Molecular docking analysis predicted a potentially favorable binding mode for conjugate **17** within the ribosomal target site; meanwhile, confocal fluorescence imaging revealed greater cellular accumulation of conjugate **17** than that of nosiheptide in *E. coli*. **Conclusions:** The siderophore–NOS conjugation strategy enabled the macromolecular thiopeptide antibiotic nosiheptide to overcome the intrinsic permeability barrier in the tested Gram-negative model strain through bacterial iron transport pathways. These findings provide a foundation for further evaluation of this strategy against a broader range of Gram-negative pathogens.

Keywords: nosiheptide; siderophores; gram-negative bacteria; drug resistance, bacterial

1. Introduction

The discovery of antibiotics revolutionized the treatment of bacterial infections and significantly reduced infection-related mortality. However, the widespread and often inappropriate use of antibiotics has accelerated the emergence and dissemination of antimicrobial resistance (AMR), which now poses a major threat to global public health. Relevant studies indicate that over 10 million annual fatalities are predicted by mid-century, with a direct link to bacterial resistance [1]. Antibiotic resistance in Gram-negative pathogens, such as *Escherichia coli* (*E. coli*), *Acinetobacter baumannii* (*A. baumannii*), *Pseudomonas aeruginosa* (*P. aeruginosa*), and *Klebsiella pneumoniae* (*K. pneumoniae*), is a cause for concern, especially since the availability of effective treatments for these pathogens is decreasing [2]. Similarly, multidrug-resistant Gram-positive pathogens such as methicillin-resistant *Staphylococcus aureus* (MRSA) and vancomycin-resistant *Enterococcus* remain a major clinical challenge, and plant-derived natural products have emerged as an important source of new antibacterial leads [3]. Resistance in these pathogens arises via three main pathways: altering the target site, modifying enzymes, or diminishing the drug's intracellular build-up caused by efflux. To date, fewer than 50 potential antibiotic candidates have entered clinical trials, and it's unexpected that only a small number of these showed effectiveness against Gram-negative pathogens. Consequently, there is a critical demand for innovative antibiotics and novel strategies to combat bacterial resistance in clinical settings [4]. In contrast to Gram-positive bacteria, Gram-negative bacteria exhibit distinct features, particularly their reduced membrane permeability resulting from their characteristic double-membrane structure. Because Gram-negative bacteria possess an outer membrane and an inner membrane, siderophores enable antibiotics to cross this membrane and counteract drug resistance via a unique iron absorption system [5]. Drug delivery mechanisms based on iron vectors, often known as the "Trojan horse" strategy (Fig. 1), could potentially surmount obstacles to bacterial drug penetration. In parallel, membrane-disrupting natural products such as nordihydroguaiaretic acid (NDGA) have shown potent antibacterial and anti-biofilm activity against

Copyright: © 2026 The Author(s). Published by IMR Press.
This is an open access article under the CC BY 4.0 license.

Publisher's Note: IMR Press stays neutral with regard to jurisdictional claims in published maps and institutional affiliations.

drug-resistant Gram-positive pathogens, although their efficacy against Gram-negative bacteria remains limited by the outer membrane barrier [6]. Siderophores are secreted by microorganisms [7]. Microorganisms produce a diverse range of siderophores to acquire iron from their surrounding environment, particularly under iron-limited conditions [8].

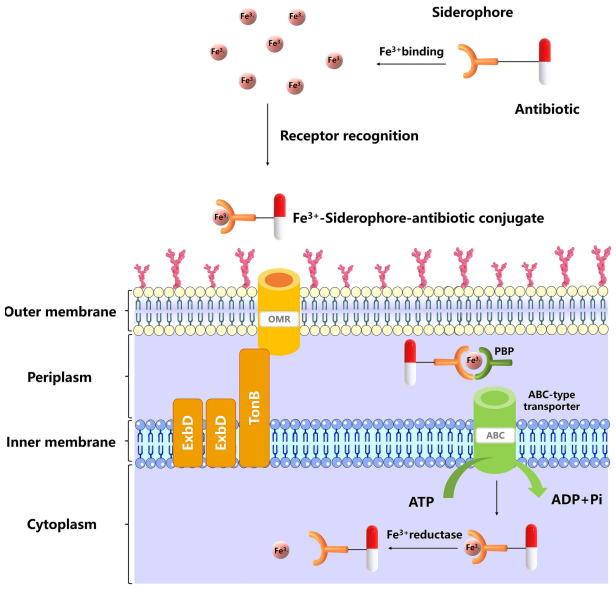


Fig. 1. The strategy of "Trojan horse". This figure was created using Microsoft PowerPoint (version 2021, Microsoft Corporation, Redmond, WA, USA).

Based on their chemical structures, siderophores can be classified into phenol, catecholate, hydroxamate, carboxylate, α-hydroxy carboxylate, and 3-hydroxypyridone [9] (Fig. 2). Most pathogens utilize siderophores for assimilation of ferric ions under iron-deficient conditions. Because iron is a necessary nutrient, siderophore uptake mechanisms of pathogens are highly activated at infection sites, which serve as effective conduits for transporting antibiotics conjugated with cognate siderophores through membrane layers.

Recently, this design of natural selection has been successfully translated into clinical applications, such as cefiderocol, the siderophore–antibiotic conjugate recently approved by the Food and Drug Administration [10]. Therefore, this study aimed to investigate the potential of catechol-based siderophore mimetics as delivery vehicles for facilitating antibiotic penetration into Gram-negative bacteria. Several studies have explored this strategy. Flanagan and co-workers [11] discovered U-78608 (**7**) (Fig. 3) to be highly effective *in vitro* against *P. aeruginosa* (minimum inhibitory concentration, MIC = 0.5 μM), yet ineffective in curing *P. aeruginosa* 1091-05 respiratory tract infections (RTI) in animal models (RTI PD50 >150 mg/kg), possibly due to its strong binding to plasma proteins.

Researchers chose various compounds, each with unique triazolone side chain characteristics, to pair with monocarbam and then synthesized and tested MC-1 (**8**). The design strategy of MC-1 focuses more on altering side chain groups, with the goal of decreasing protein attachment and enhancing pulmonary permeability. MC-1 exhibits superior MIC (0.125 μM) and RTI PD50 (20.7 mg/kg) in combating *P. aeruginosa*. To enhance its stability, scientists inserted a methyl at the C4 spot in the β-lactam ring of MC-1, resulting in a more stable MC-1 analogue (**9**) in alkaline environments. Analysis of the relationship between structure and activity revealed that the orientation of the triazolone conjugate's side chain and the presence of hydrogen bond donors had a notable impact on the outcomes in a living organism. Murphy-Benenato and co-workers [12] designed a novel form of siderophore–monocarbam conjugate (**10**). Research revealed that substituting the siderophore with 1,3-dihydroxypyridone enhances the compound's effectiveness and physical characteristics, and by altering its structure, this novel conjugate variant exhibits strong activity (MIC_{50} = 0.5 μg/mL, MIC_{90} = 2 μg/mL). Paulen and co-workers [13] reported the synthesized catechol-oxazolidinone conjugate (**5**). The efficacy of conjugate **11** in combating *P. aeruginosa* PAO1 (MIC = 128–512 μM) notably surpassed that of linezolid (MIC >1024 μM). Goldberg et al. [14] discovered that the emerging pyrazolidone antibiotic YU253434 (**12-1**), resembling the siderophore of γ-lactam, demonstrated effective inhibitory properties against 197 *P. aeruginosa* clinical isolates, with a minimum inhibitory concentration (MIC_{50} = 1 μM, MIC_{90} = 8 μM) surpassing that found in existing clinical β-lactam medications. It remains stable against β-lactamase. On this basis, researchers synthesized the chloramothiazole analogue YU253911 [15] (**12-2**) of **12-1**. The study revealed that the MIC_{50} of **12-2** for combating 23 kinds of multidrug-resistant (MDR) *P. aeruginosa* was measured at 0.5 μg/mL, exhibiting a dose-responsive effectiveness in mouse models of thigh infection. Liu and co-workers [16] conducted extensive structure-activity relationship and structure-metabolism relationship (SMR) studies and discovered a promising cefiderocol analog, YFJ-36, which features a new thioether linker. Compared with cefiderocol, YFJ-36 showed broad-spectrum antibacterial activity against *E. coli* and resistant *Acinetobacter baumannii* A (MIC = 0.05–0.6 μg/mL).

Herein, we prepared a bidentate catechol siderophore–NOS conjugate (**17**) and characterized its pharmacological properties in *P. aeruginosa* PAO1 as a proof-of-concept Gram-negative model. As a thiopeptide antibiotic, nosiheptide (NOS) exhibited nanomolar potency against diverse Gram-positive bacteria [17], including methicillin-resistant *Staphylococcus aureus* (MRSA) and vancomycin-resistant *Enterococcus faecium* (VRE); however, its high molecular weight makes it difficult to penetrate the outer membrane barrier of Gram-negative bacteria. The cate-

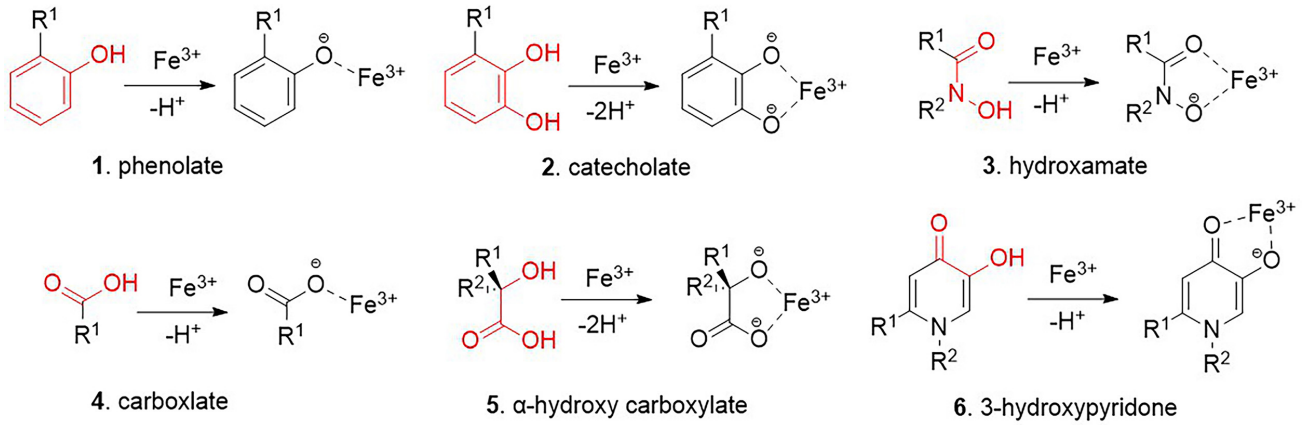


Fig. 2. Structural units of siderophore and functional (1–6). The chemical structures were drawn using ChemDraw (version 21.0.0, PerkinElmer Informatics, Waltham, MA, USA).

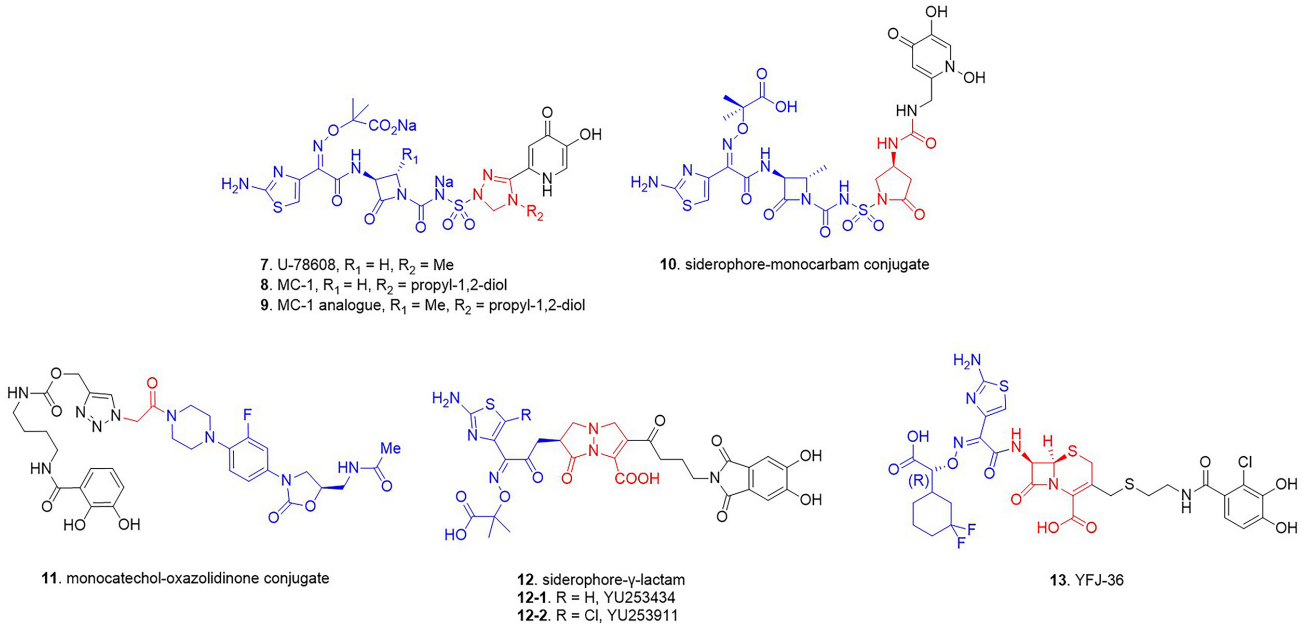


Fig. 3. Structures of siderophore–antibiotic conjugates (7–13).

chol siderophore–NOS conjugate showed increased activity against the tested Gram-negative model strain. Under iron-limited conditions, its antibacterial activity was markedly enhanced (MIC = 64 μM in casamino acid (CAA) vs. 256 μM in Mueller-Hinton II broth (MHB)), indicating that bacterial iron acquisition pathways contribute to its uptake. Analysis using a transporter-deficient mutant strain suggested that *PfeA* alone is not essential for conjugate uptake, indicating that additional iron acquisition pathways may contribute to the internalization of conjugate **17**. This research revealed that by linking a simple catechol siderophore and thereby circumventing the permeability barrier typical of Gram-negative bacteria, antibiotics normally used for Gram-positive infections can be adapted to the tested Gram-negative model strain, providing a basis for broader spectrum expansion in future work.

2. Material and Methods

2.1 General Information

All solvents were commercially available, with a purity of 99.9%. Water and chromatographic acetonitrile served as the mobile phases. The processes of separation and purification utilized the Dionex semi-preparative HPLC. The semi-preparative chromatographic columns utilized were SB-C_{18} types. The process of column chromatography purification utilized Merck silica gel 60 (63–200 μm). nuclear magnetic resonance (NMR) spectra were recorded using a Bruker AVANCE 400 MHz spectrometer, featuring chemical shifts in ppm and solvent peaks ($CDCl_3$ 7.24 ppm, $(CD_3)_2CO$ 2.05 ppm, D_2O 4.79 ppm). To prepare NMR samples of conjugate **17**, 5 mg of the analyte was dissolved in a solution of 0.7 mL deuterated chloroform and deuterated methanol in a 9:1 ratio, while the rest

of the compound samples were made using deuterated acetone or deuterated water. The values for chemical shifts are measured in parts per million, in comparison to the internal benchmark tetramethylsilane (TMS), and the coupling constants (J) are expressed in hertz (Hz). The School of Chemistry and Chemical Engineering at Shandong University utilized an Orbitrap IQ-X device to capture high-resolution mass spectrometry (HRMS) spectra. Pre-coated silica gel GF-254 (Merck, Germany) was used to conduct thin-layer chromatography. Observations of spots were conducted with ultraviolet (UV) light at wavelengths of 254 nm and 365 nm.

2.2 The Synthesis of Siderophore Mimetic (15a)

The 3,4-dihydroxybenzoic acid (400 mg, 2.59 mmol) was mixed in 10 mL N,N-dimethylformamide (DMF). Next, PyAOP (1350 mg, 2.59 mmol) and N,N-diisopropylethylamine (DIPEA, 417 mg, 3.23 mmol) were introduced into it, and the mixture was stirred at room temperature for 10 min. Subsequently, N-Boc-1,2-ethylenediamine (415 mg, 2.59 mmol) was introduced into the mixture, which underwent magnetic stirring at 30 °C and 1500 rpm for a duration of 16 h. The mixture for the reaction was transferred into 200 mL of water, underwent three extractions using ethyl acetate, and then the extracts were merged and rinsed twice with water. Following the use of anhydrous Na_2SO_4 for water extraction, the solvent was evaporated under reduced pressure, and column chromatography (ethyl acetate-hexane = 15:1) was employed to purify the product, resulting in the formation of compound **15a** as a white solid with an 86% yield. ^{1}H NMR (400 MHz, $(CD_3)_2CO$): δ 8.71 (s, 2H), 7.96 (t, J = 5.5 Hz, 1H), 7.52 (d, J = 2.2 Hz, 1H), 7.33 (dd, J = 8.2, 2.2 Hz, 1H), 6.87 (d, J = 8.3 Hz, 1H), 6.45 (t, J = 5.9 Hz, 1H), 3.50 (q, J = 5.9 Hz, 2H), 3.33 (q, J = 6.1 Hz, 2H), 1.39 (s, 9H).

2.3 The Synthesis of Siderophore Mimetic (15b)

Similar to the process in **15a**, the synthesis technique involved altering the reaction raw material to N-boc-1,3-propanediamine (451 mg, 2.59 mmol), followed by purification through column chromatography (ethyl acetate-hexane = 15:1), resulting in the production of compound **15b** as a white solid with an 88% yield. ^{1}H NMR (400 MHz, $(CD_3)_2CO$): δ 8.37 (s, 2H), 7.72 (s, 1H), 7.47 (d, J = 2.3 Hz, 1H), 7.32 (dd, J = 8.2, 2.2 Hz, 1H), 6.87 (d, J = 8.3 Hz, 1H), 6.20 (s, 1H), 3.43 (q, J = 6.4 Hz, 2H), 3.17 (q, J = 6.4 Hz, 2H), 1.71 (p, J = 6.5 Hz, 2H), 1.42 (s, 9H).

2.4 The Synthesis of Siderophore Mimetic (15c)

Similar to the process in **15a**, the synthesis technique involved altering the reaction raw material to N-Boc-1,4-butanediamine (487 mg, 2.59 mmol), followed by purification through column chromatography (ethyl acetate-hexane = 15:1), resulting in the production of compound **15c** as a white solid with an 82% yield. ^{1}H NMR (400 MHz, $(CD_3)_2SO$): δ 9.46 (s, 1H), 9.12 (s, 1H), 8.15 (t, J = 5.7 Hz, 1H), 7.30 (d, J = 2.1 Hz, 1H), 7.20 (dd, J = 8.2, 2.1 Hz, 1H), 6.84 (t, J = 5.6 Hz, 1H), 6.77 (d, J = 8.2 Hz, 1H), 3.26–3.17 (m, 2H), 2.95 (q, J = 6.1, 5.6 Hz, 2H), 1.57 – 1.41 (m, 4H), 1.40 (s, 9H).

2.5 The Synthesis of Siderophore Mimetic (15d)

Similar to the process in **15a**, the synthesis technique involved altering the reaction raw material to N-Boc-1,5-cadaverine (523 mg, 2.59 mmol), followed by purification through column chromatography (ethyl acetate-hexane = 15:1), resulting in the production of compound **15d** as a white solid with an 80% yield. ^{1}H NMR (400 MHz, D_2O): δ 7.21 (s, 1H), 7.11 (d, J = 7.6 Hz, 1H), 6.71 (d, J = 8.1 Hz, 1H), 3.32–3.14 (m, 4H), 2.92 (d, J = 7.3 Hz, 2H), 1.50 (t, J = 8.0 Hz, 2H), 1.41–1.38 (m, 2H), 1.31 (s, 9H).

2.6 The Synthesis of Siderophore–NOS Conjugate (17)

25 mg (0.02 mmol) of NOS was mixed into 4 mL of dichloromethane-methanol in a 3:1 ratio. The **15a** (0.4 mmol, 118 mg) was dissolved in a 5:1 ratio of DCM-TFA (4 mL) and left to react at room temperature for 3 h (a significant excess of the **15a** was used to drive the Michael addition reaction to completion). Subsequently, the solvent was distilled off under reduced pressure, followed by the addition of 5 mL of ethyl acetate to dissolve the reactants, and the pH was modified to a range of 7–8 using a saturated Na_2CO_3 solution, before evaporation under a lower pressure to form a solid. The substance was mixed with 8 mL of methanol, passed through a filtration process, then gathered and incorporated into the NOS solution. The process was conducted at a temperature of 30 °C and a stirring speed of 1500 rpm over a duration of 24 h. Through evaporation in a low-pressure environment, the solvent was eliminated, followed by purification of the residue using preparative high-performance liquid chromatography (HPLC), resulting in the formation of conjugate **17** as a yellow solid with a 45% yield. ^{1}H NMR (400 MHz, $CDCl_3$-MeOH, 9:1): δ = 1.24 (bd, J = 6.6 Hz, 3H), 1.75 (d, J = 6.0 Hz, 2H), 2.01 (d, J = 3.6 Hz, 3H), 2.23 (s, 1H), 2.43 (t, J = 6.6 Hz, 1H), 2.46 (d, J = 6.6 Hz, 2H), 2.50 (s, 3H), 3.38–3.52 (m, 3H), 3.70 (m, 1H), 4.09 (m, 1H), 4.20 (d, J = 12.0 Hz, 1H), 4.49 (s, 1H), 5.08 (d, J = 9.0 Hz, 1H), 5.80–5.83 (m, 1H), 5.90 (d, J = 10.8 Hz, 1H), 6.02 (bs, 1H), 6.38 (q, J = 7.2 Hz, 1H), 6.71 (J = 6 Hz, 1H), 6.73 (s, 1H), 6.91 (d, J = 7.2 Hz, 1H), 7.04 (q, J = 7.2 Hz, 1H), 7.18 (d, J = 7.2 Hz, 1H), 7.46 (t, J = 7.8 Hz, 1H), 7.55 (d, J = 10.2 Hz, 1H), 7.69 (s, 1H), 7.70 (s, 1H), 7.86 (d, J = 14.4 Hz, 1H), 7.97 (d, J = 1.2 Hz, 1H), 8.01 (s, 1H), 8.23 (s, 1H), 8.32 (s, 1H), 8.52 (s, 1H). All OH-and several NH groups were not observed due to hydrogen/deuterium (H/D) exchange. HRMS: calcd for $C_{60}H_{56}N_{15}O_{15}S_6^+$ $[M+H]^+$ 1418.2406 (**Supplementary Fig. 1**).

2.7 Antimicrobial Susceptibility Testing

To assess the efficacy of compounds, they were diluted in a two-fold series using MHB and a CAA medium lacking iron (medium composition: 5 g L^{-1} [(low-iron-CAA); Difco], 1.46 g L^{-1} $K_2HPO_4 \cdot 3H_2O$, 0.25 g L^{-1} $MgSO_4 \cdot 7H_2O$), maintaining an inoculum of 1 × 10^5 CFU/mL. MIC values represent the lowest concentration required to inhibit bacterial proliferation following an 18 h (MHB) or 48 h (CAA) incubation at 37 °C. The creation of the PAO1Δ*pfeA* mutant followed methods reported earlier with slight modifications [13], amplification of PCR segments adjacent to *pfeA* was achieved from the genomic DNA of *P. aeruginosa* PAO1, employing primer pairs Δ*pfeA*#1/Δ*pfeA*#2 (5′-AACATGAATTCAGCTGGCCCAGGCCCTG-3′/5′-TGAGGACATCGGTGATCTCCG-3′) and Δ*pfeA*#3/Δ*pfeA*#4 (5′-TCACCGATGTCCTCACGCTATACCAGCCTGACCGCGTC-3′/5′-AACATAAGCTTAGGCCGTCGAGCGGCTG-3′). The two segments were combined, and a 1400 bp segment was amplified with primer pairs Δ*pfeA*#1/Δ*pfeA*#4, then inserted into the suicide plasmid pME3088 through EcoRI and HindIII restriction sites, resulting in the creation of pME3088Δ*pfeA*. The removal of *P. aeruginosa*'s chromosomal *pfeA* gene was accomplished by transferring pME3088Δ*pfeA* from *E. coli* TOP10 to the PAO1 wild-type strain, followed by plasmid integration into this chromosome to enhance resistance to tetracycline. A subsequent crossing-over event removed the vector, yielding the PAO1Δ*pfeA* mutant. The excised genetic strain underwent confirmation through PCR and sequencing techniques.

2.8 Iron Competition Assay

To investigate the iron-regulated uptake mechanism of conjugate **17**, MIC values were determined in CAA medium supplemented with different concentrations of Fe^{3+}. Briefly, bacterial suspensions were prepared in CAA medium containing Fe^{3+} at final concentrations of 0, 1, 10, and 100 μM. NOS and conjugate **17** were serially diluted and added to the bacterial cultures. After incubation at 37 °C for 24 h, MIC values were determined according to the standard broth microdilution method. All experiments were performed in triplicate.

2.9 Outer Membrane Permeability Assay

To evaluate the contribution of the outer membrane barrier to antibacterial activity, MIC values were determined in the presence of sub-inhibitory concentrations of polymyxin B nonapeptide (PMBN, 2 μg/mL) or ethylenediaminetetraacetic acid (EDTA, 50 μM). Bacterial cultures were treated with NOS or conjugate **17** in CAA medium supplemented with PMBN or EDTA, and MIC values were determined using the broth microdilution method.

2.10 Molecular Docking Simulation

In this research, we employed a semi-flexible docking technique to create a stable complex. The AutoDock Vina 1.1.2 program facilitated the molecular docking of NOS, conjugate **17**, and protein 2ZJP (PDB ID: 2ZJP). The PyMOL 2.4 software facilitated the completion of protein pre-processing, involving the removal of water molecules, surplus ligands, and the addition of hydrogen atoms. AutoDockTools 1.5.6 facilitated the creation of PDBQT files tailored for docking simulations. The dimensions of the 2ZJP protein docking box measured 32 Å × 38 Å × 68 Å, arranged in a 1.00 Å grid. The center coordinates of the docking box were: x:y:z = 133.932:70.251:99.943. The remaining parameters continued to be set to their preset values. Docking outcomes were adjusted to display the top 9 docking locations. The docking structure characterized by minimal binding energy and the greatest frequency of clustering is deemed the most likely mode of interaction between the ligand and the protein. Ultimately, the docking outcomes were visualized using PLIP and PyMOL 2.4 software. Through this method, the ligand binding to the receptor becomes visible, allowing us to delve deeper into the complex's stability and interplay.

2.11 Imaging of Drug Delivery Efficacy

Due to its large molecular weight, NOS has difficulty penetrating the bacterial outer membrane. To investigate whether siderophore conjugation could enhance the bacterial uptake of NOS, *E. coli* cells were stained with Rhodamine B (red fluorescence), which was prepared as a stock solution at a concentration of 10 mg/mL. Subsequently, the bacterial cells were separately incubated with Cy5-labeled NOS and Cy5-labeled conjugate **17** (10 μM each) for 2 h. After incubation, the cells were washed with PBS to remove unbound fluorescent dyes and compounds. Fluorescence images were acquired using a confocal laser scanning microscope.

3. Results

3.1 Synthesis of Siderophore–NOS Conjugate

3,4-Dihydroxybenzoic acid (**14**) was selected as the catecholate siderophore building block, and aliphatic amines (**R1**) were introduced as iron-binding groups to synthesize catecholate siderophore mimetics (**15a–15d**) using PyAOP-mediated coupling (Fig. 4). After purification and Boc deprotection with trifluoroacetic acid (TFA), the target compounds **15a–15d** were obtained in yields of 86%, 88%, 82%, and 80%, respectively. The siderophore–NOS conjugate was synthesized by linking the siderophore mimetic to the dehydroalanine-containing NOS scaffold through a Michael addition reaction (Fig. 5). Among the synthesized mimetics, **15a** and **15b** differed only by one methylene group; therefore, **15a**, containing the shorter linker,

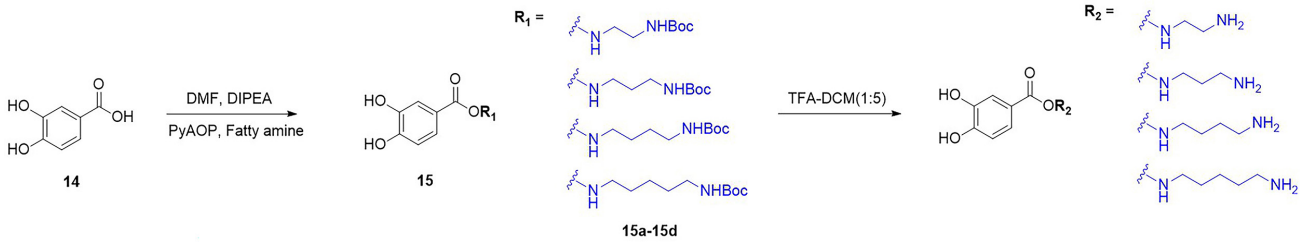


Fig. 4. Synthesis route of siderophore mimetics (15a–15d).

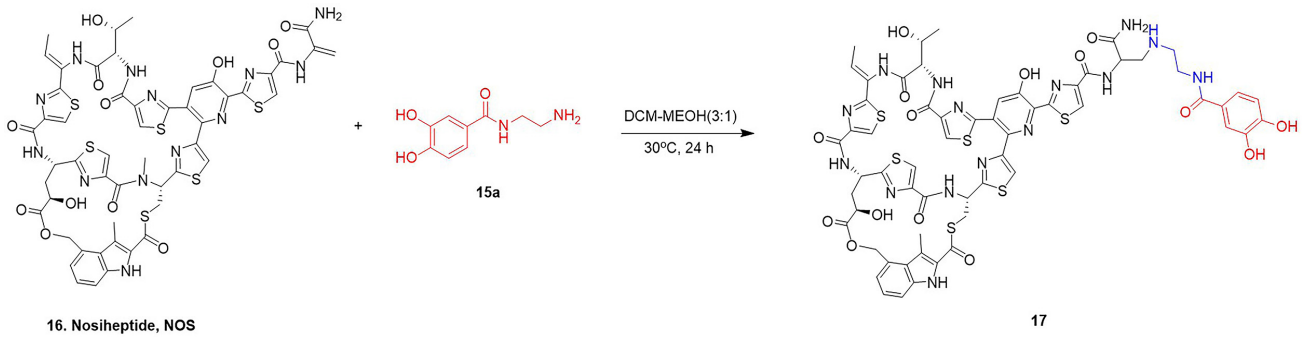


Fig. 5. Synthesis route of siderophore–NOS conjunjugate (17).

was selected for conjugation. The desired conjugate **17** was obtained in 45% yield.

3.2 Antibacterial Activity Against P. aeruginosa PAO1

The antibacterial activities of siderophore mimetics (**15a–15d**), NOS (**16**), and final conjugate **17** were evaluated against *Pseudomonas aeruginosa* PAO1 under iron-deficient (CAA) and iron-rich (MHB) conditions. The activity of **17** was further investigated using a *P. aeruginosa* PAO1 mutant lacking the outer membrane transporter gene *pfeA* (PAO1Δ*pfeA*). MIC values were determined using the broth microdilution method. NOS showed no detectable antibacterial activity under either condition, with MIC values >1024 μM in both CAA and MHB media. The siderophore mimetics (**15a–15d**) showed no antibacterial activity in either medium and instead promoted bacterial growth. In contrast, conjugate **17** displayed enhanced antibacterial activity under iron-limited conditions, with an MIC value of 64 μM in CAA medium. Its activity decreased under iron-rich conditions, with an MIC value of 256 μM in MHB medium. The antibacterial activity of **17** against PAO1Δ*pfeA* was comparable to that against wild-type PAO1 (Table 1). In addition, to confirm the iron-regulated uptake mechanism, MIC values of conjugate **17** were determined in CAA medium with increasing Fe^{3+} concentrations (0, 1, 10, and 100 μM). The activity of conjugate **17** decreased progressively with increasing Fe^{3+} (MIC: 64, 64, 128, and 256 μM), whereas NOS remained inactive (>1024 μM) under all conditions (**Supplementary Table 1**). These results support the involvement of iron-regulated uptake pathways in the antibacterial activity of conjugate **17**. Furthermore, to investigate the role of the outer membrane barrier, MIC values were determined with sub-inhibitory PMBN (2 μg/mL) and EDTA (50 μM). NOS alone showed no activity (>1024 μM), but its MIC decreased to 128 μM (PMBN) and 64 μM (EDTA). In contrast, conjugate **17** remained unchanged (64 μM) under all conditions (**Supplementary Table 2**). These results confirm that the outer membrane barrier is the primary limitation for NOS against Gram-negative bacteria. Next, to evaluate whether siderophore conjugation enhanced the bactericidal activity of NOS, time-kill assays were performed against *P. aeruginosa* PAO1 under iron-limited conditions (**Supplementary Fig. 2** and **Supplementary Table 3**). NOS showed negligible killing activity at the same concentrations as conjugate **17** (64, 128, and 256 μM, corresponding to 1×, 2×, and 4× MIC of conjugate **17**). In contrast, conjugate **17** exhibited concentration-dependent bactericidal activity, with higher concentrations showing faster bacterial reduction. These findings indicate that siderophore conjugation enhances the antibacterial activity of NOS, potentially by facilitating bacterial uptake and improving intracellular drug delivery.

3.3 Molecular Docking Analysis

Molecular docking analysis was performed to investigate the possible binding modes of NOS and conjugate **17** with the 23S rRNA region of the 50S ribosomal subunit (PDB ID: 2ZJP). Conjugate **17** exhibited a distinct predicted binding pose compared with NOS (Fig. 6). The predicted binding energy of conjugate **17** was –9.1 kcal/mol, compared with –6.5 kcal/mol for NOS (Table 2), sug-

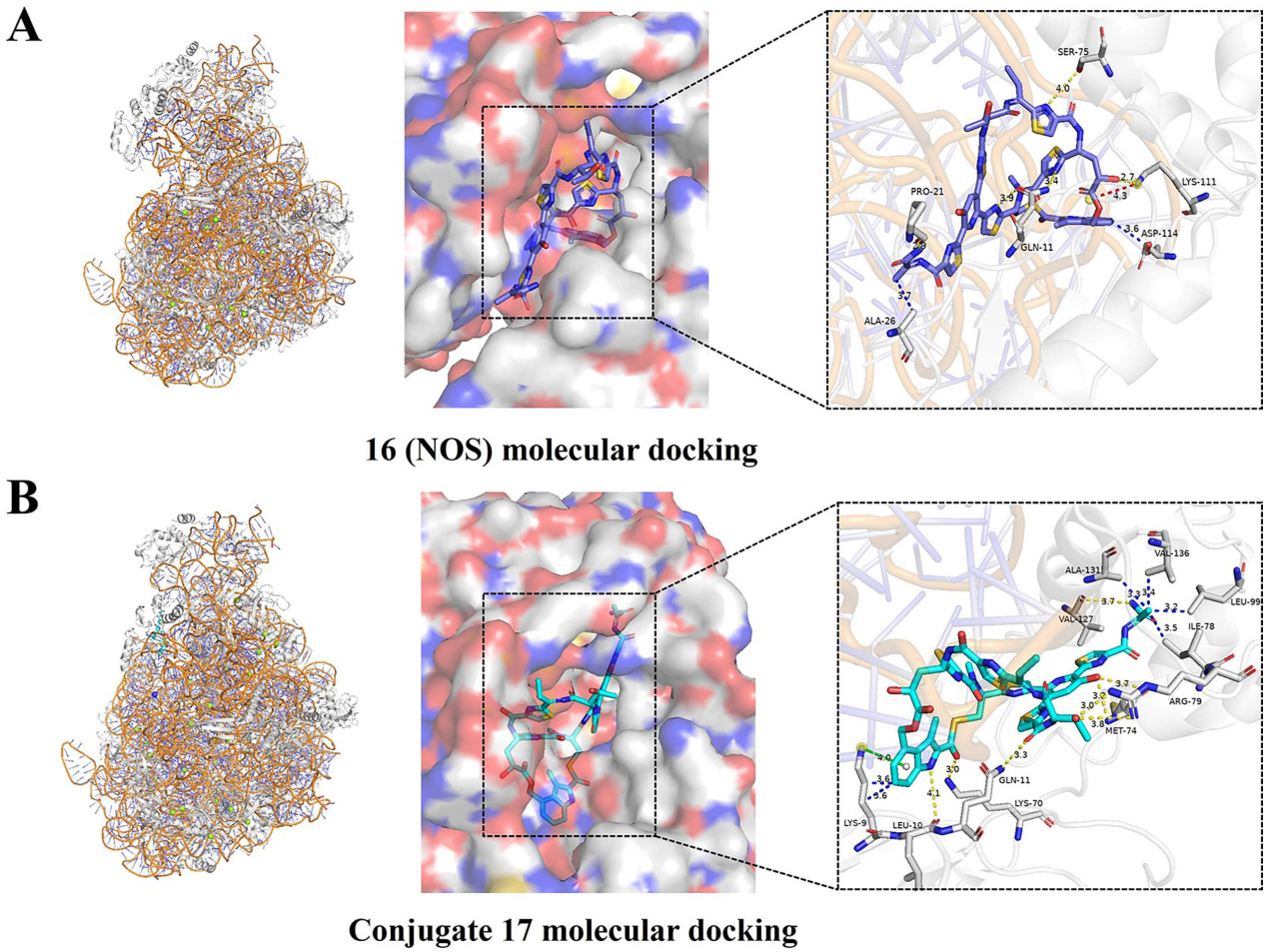


Fig. 6. Molecular docking analysis. 2ZJP as receptor, **16** (NOS) (A) and conjugate **17** (B) as ligands. Hydrogen bonds, hydrophobic interactions, salt bridges, and π–π stacking interactions are represented in yellow, blue, red, and green, respectively.

Table 1. MIC (μM) of siderophore mimetics (15a–15d), NOS (16), and conjugate 17 against *P. aeruginosa* PAO1 and PAO1Δ*pfeA* in iron-limited (CAA) and iron-rich (MHB) media.

Compounds	PAO1 CAA	PAO1 MHB	PAO1Δ*pfeA* CAA
15a	>1024	>1024	>1024
15b	>1024	>1024	>1024
15c	>1024	>1024	>1024
15d	>1024	>1024	>1024
16 (NOS)	>1024	>1024	>1024
17	64	256	64

CAA, casamino acid; MHB, Mueller-Hinton II broth.

gesting a potentially more favorable interaction profile for conjugate **17** within the modeled binding site. However, this computational result should be interpreted only as a possible binding mode and does not by itself demonstrate enhanced target engagement or antibacterial activity. The docking results suggested that hydrophobic interactions, hydrogen bonding, and π–π stacking interactions may contribute to the stabilization of conjugate binding.

Table 2. Docking scores of NOS and conjugate 17.

Compounds	Binding energy (kcal/mol)
16 (NOS)	–6.5
17	–9.1

3.4 Bacterial Uptake Analysis

To evaluate bacterial uptake, *E. coli* membranes were stained with Rhodamine B, while conjugate **17** and NOS were labeled with Cy5. Confocal fluorescence imaging revealed stronger cell-associated fluorescence signals for conjugate **17** than for NOS, suggesting enhanced bacterial association and/or uptake (Fig. 7). To exclude the possibility that Cy5 labeling affected antibacterial activity, MIC values of Cy5-labeled NOS and Cy5-labeled conjugate **17** were determined and compared with those of the unlabeled compounds. Cy5 labeling did not significantly change the MIC values (**Supplementary Table 4**), confirming that the enhanced fluorescence signal of conjugate **17** reflects increased bacterial uptake.

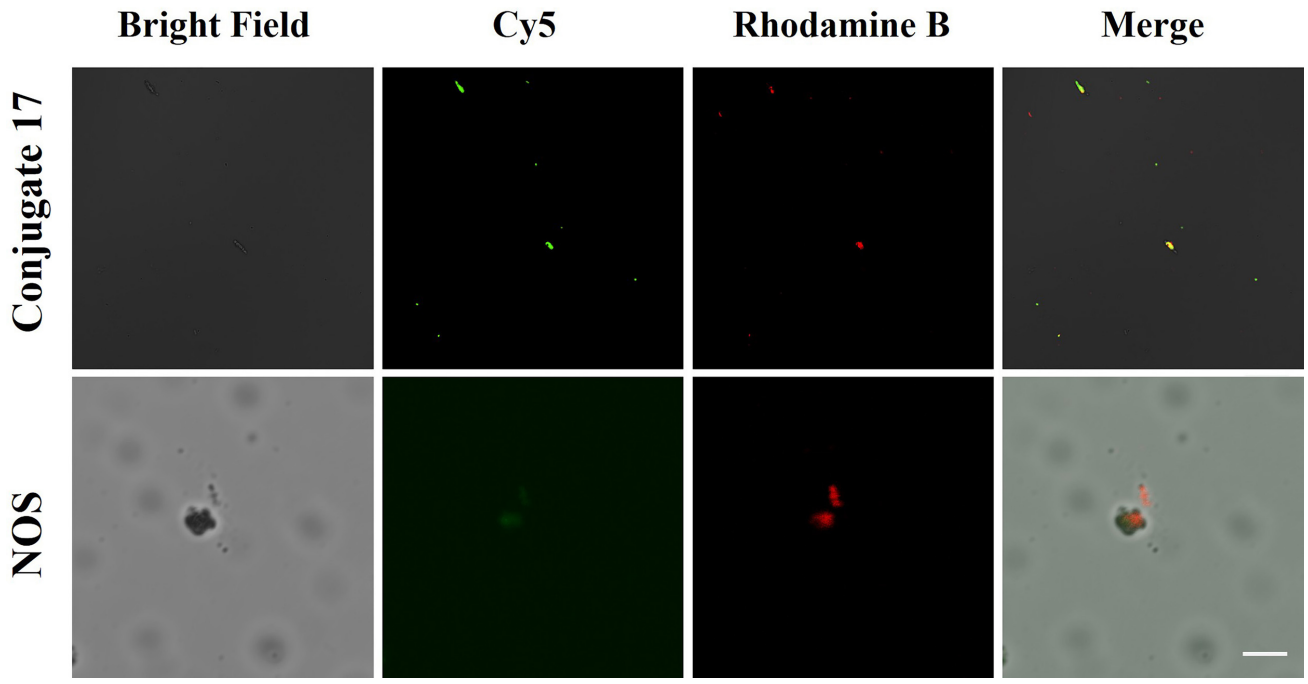


Fig. 7. Representative confocal fluorescence images of *E. coli* (stained with Rhodamine B) treated with Cy5-labeled conjugate 17 and NOS for 2 h. Scale bar: 20 μm.

4. Discussion

The synthetic results demonstrated that PyAOP provided an efficient strategy for preparing catecholate siderophore mimetics, with improved reaction efficiency and fewer by-products compared with HOBt-mediated coupling. The successful preparation of conjugate **17** confirmed the feasibility of employing siderophore mimetics as delivery components for NOS.

The antibacterial results revealed that conjugate **17** exhibited iron-dependent activity. The increased potency under iron-limited conditions and reduced activity in iron-rich medium suggest that bacterial iron acquisition pathways may contribute to the uptake and activity of **17**. However, deletion of *pfeA* did not significantly affect the antibacterial activity of **17**, suggesting that conjugate **17** uptake may involve multiple or redundant iron acquisition pathways rather than a single transporter. The siderophore moiety enhanced the biological performance of NOS by improving bacterial uptake. Unlike NOS, which showed no detectable activity against *P. aeruginosa* PAO1 due to poor outer membrane permeability, conjugate **17** achieved cell-associated fluorescence through siderophore-mediated delivery, thereby improving antibacterial activity. Molecular docking analysis was performed to explore the possible binding modes of NOS and conjugate **17** within the 23S rRNA region of the 50S ribosomal subunit. Conjugate **17** was predicted to adopt a more favorable binding pose than NOS, with the additional aromatic group of the siderophore moiety potentially contributing to π–π stacking, hydrophobic interactions, and hydrogen bonding. These findings suggest that siderophore conjugation is sterically compatible with ribosomal target binding and may therefore not compromise the intrinsic ribosome-targeting activity of NOS. However, as a computational approach, docking provides only a static prediction of binding poses and cannot be regarded as direct evidence of enhanced ribosomal inhibition. The improved antibacterial activity of conjugate **17** is supported by the experimentally observed siderophore-mediated uptake, including its iron-dependent MIC shift and enhanced intracellular accumulation. It should be emphasized that this study was a mechanistic proof-of-concept investigation in a single model strain, *P. aeruginosa* PAO1. Although *E. coli* was used in the uptake imaging experiments, no MIC data were obtained for *E. coli*, *K. pneumoniae*, or *A. baumannii*. Therefore, the conclusions here establish the feasibility of the siderophore–NOS strategy in the tested model strain, rather than broad-spectrum activity. Systematic evaluation across diverse clinical Gram-negative isolates, including multidrug-resistant strains, will be addressed in a follow-up study. Overall, in the tested *P. aeruginosa* PAO1 model, conjugate **17** combines siderophore-mediated bacterial uptake with the ribosome-targeting activity of NOS, providing a strategy to overcome the limited permeability of large antibacterial molecules against Gram-negative bacteria.

5. Limitations

This study was primarily based on *in vitro* evaluations, and further investigations in animal models are required to assess the pharmacological properties and therapeutic po-

tential of conjugate **17**. Previous pharmacokinetic investigations of antibiotic–phytochemical conjugates have highlighted that favorable *in vitro* antimicrobial activity does not necessarily translate into adequate systemic drug exposure, underscoring the importance of pharmacokinetic optimization during further development [18]. Moreover, preliminary cytotoxicity evaluation in mammalian cell models and comprehensive safety assessments will be necessary in future studies to further evaluate the therapeutic potential of conjugate **17**. Optimization of the synthetic route is also needed to improve the overall yield and facilitate future development. Furthermore, the antibacterial activity of conjugate **17** was systematically profiled only in *P. aeruginosa* PAO1. To improve the generalizability of the present findings, future work should extend the evaluation to other clinically relevant Gram-negative pathogens such as *E. coli*, *K. pneumoniae*, and *A. baumannii*. Such broader species coverage, together with testing against multidrug-resistant clinical isolates, will be necessary before any general claim regarding activity against Gram-negative pathogens can be made.

6. Conclusion

In this study, a bidentate catechol siderophore–NOS conjugate (**17**) was successfully synthesized to overcome the permeability limitation of nosiheptide in *P. aeruginosa* PAO1. By exploiting bacterial iron uptake pathways, conjugate **17** exhibited enhanced antibacterial activity under iron-limited conditions and improved cellular uptake compared with the parent antibiotic in the tested model strain. These findings demonstrate the feasibility of siderophore conjugation as a strategy for improving the antibacterial activity of thiopeptide antibiotics and warrant further investigation, including safety evaluation and *in vivo* studies.

Availability of Data and Materials

The datasets used and analyzed during the current study are available from the corresponding author on reasonable request.

Author Contributions

SZ: Writing-review and editing, Data curation, Funding acquisition. JL: Investigation. JJ: Writing-Original draft, Resources, Investigation. CL: Conceptualization, Methodology, Writing-Original draft. All authors contributed to editorial changes in the manuscript. All authors read and approved the final manuscript. All authors have participated sufficiently in the work and agreed to be accountable for all aspects of the work.

Ethics Approval and Consent to Participate

This study did not involve human participants or animal subjects. All bacterial strains used in this study were handled in accordance with the Chinese national standard General Requirements for Laboratory Biosafety (GB 19489—2008) and relevant institutional biosafety regulations. Therefore, ethical approval from an ethics committee was not required.

Acknowledgment

Not applicable.

Funding

This research received no external funding.

Conflicts of Interest

The authors declare no conflicts of interest.

Supplementary Material

Supplementary material associated with this article can be found, in the online version, at https://doi.org/10.31083/Pharmazie56395.

References

[1] Rayner B, Verderosa AD, Ferro V, Blaskovich MAT. Siderophore conjugates to combat antibiotic-resistant bacteria. RSC Medicinal Chemistry. 2023; 14: 800–822. https://doi.org/10.1039/d2md00465h

[2] Kim DY, Yeom S, Park J, Lee H, Kim HJ. Cytoplasmic Delivery of an Antibiotic, Trimethoprim, with a Simple Bidentate Catechol Analog as a Siderophore Mimetic. ACS Infectious Diseases. 2023; 9: 554–566. https://doi.org/10.1021/acsinfecdis.2c00556

[3] Lou S, Jin W, He M, Dai C, Zhu Z, Li P, et al. Dehydroeffusol from Juncus effusus L. exhibits antibacterial activity against methicillin-resistant Staphylococcus aureus in vitro and in vivo. International Journal of Medical Microbiology: IJMM. 2026; 322: 151696. https://doi.org/10.1016/j.ijmm.2025.151696

[4] Mulani MS, Kamble EE, Kumkar SN, Tawre MS, Pardesi KR. Emerging Strategies to Combat ESKAPE Pathogens in the Era of Antimicrobial Resistance: A Review. Frontiers in Microbiology. 2019; 10: 539. https://doi.org/10.3389/fmicb.2019.00539

[5] Liu C, Wang W, Wang S. Siderophore-Antibiotic Conjugates: Applications of the 'Trojan horse' Strategy in Anti-Gram-Negative Bacteria Infection. Acta Chimica Sinica. 2024; 82: 1086–1108. https://doi.org/10.6023/A24070222 (In Chinese)

[6] Nikaido H. Molecular basis of bacterial outer membrane permeability revisited. Microbiology and Molecular Biology Reviews. 2003; 67: 593–656. https://doi.org/10.1128/MMBR.67.4.593-656.2003

[7] Kong H, Cheng W, Wei H, Yuan Y, Yang Z, Zhang X. An overview of recent progress in siderophore-antibiotic conjugates. European Journal of Medicinal Chemistry. 2019; 182: 111615. https://doi.org/10.1016/j.ejmech.2019.111615

[8] Soares MP, Weiss G. The Iron age of host-microbe interactions. EMBO Reports. 2015; 16: 1482–1500. https://doi.org/10.15252/embr.201540558

[9] Liu J, Hou J, Meng Y, Miao Z, Lin J, Chen W. Research Progress of Antibiotics Conjugated with Siderophores. Chinese Journal of Organic Chemistry. 2020; 40: 3026–3043. https://doi.org/10.6023/cjoc202006042 (In Chinese)

[10] Aoki T, Yoshizawa H, Yamawaki K, Yokoo K, Sato J, Hisakawa S, et al. Cefiderocol (S-649266), A new siderophore cephalosporin exhibiting potent activities against Pseudomonas aeruginosa and other gram-negative pathogens including multi-

drug resistant bacteria: Structure activity relationship. European Journal of Medicinal Chemistry. 2018; 155: 847–868. https://doi.org/10.1016/j.ejmech.2018.06.014

[11] Flanagan ME, Brickner SJ, Lall M, Casavant J, Deschenes L, Finegan SM, et al. Preparation, gram-negative antibacterial activity, and hydrolytic stability of novel siderophore-conjugated monocarbam diols. ACS Medicinal Chemistry Letters. 2011; 2: 385–390. https://doi.org/10.1021/ml200012f

[12] Murphy-Benenato KE, Bhagunde PR, Chen A, Davis HE, Durand-Réville TF, Ehmann DE, et al. Discovery of efficacious Pseudomonas aeruginosa-targeted siderophore-conjugated monocarbams by application of a semi-mechanistic pharmacokinetic/pharmacodynamic model. Journal of Medicinal Chemistry. 2015; 58: 2195–2205. https://doi.org/10.1021/jm501506f

[13] Paulen A, Gasser V, Hoegy F, Perraud Q, Pesset B, Schalk IJ, et al. Synthesis and antibiotic activity of oxazolidinone-catechol conjugates against Pseudomonas aeruginosa. Organic & Biomolecular Chemistry. 2015; 13: 11567–11579. https://doi.org/10.1039/c5ob01859e

[14] Goldberg JA, Nguyen H, Kumar V, Spencer EJ, Hoyer D, Marshall EK, et al. A γ-Lactam Siderophore Antibiotic Effective against Multidrug-Resistant Gram-Negative Bacilli. Journal of Medicinal Chemistry. 2020; 63: 5990–6002. https://doi.org/10.1021/acs.jmedchem.0c00255

[15] Goldberg JA, Kumar V, Spencer EJ, Hoyer D, Marshall SH, Hujer AM, et al. A γ-lactam siderophore antibiotic effective against multidrug-resistant Pseudomonas aeruginosa, Klebsiella pneumoniae, and Acinetobacter spp. European Journal of Medicinal Chemistry. 2021; 220: 113436. https://doi.org/10.1016/j.ejmech.2021.113436

[16] Liu F, Kou Q, Li H, Cao Y, Chen M, Meng X, et al. Discovery of YFJ-36: Design, Synthesis, and Antibacterial Activities of Catechol-Conjugated β-Lactams against Gram-Negative Bacteria. Journal of Medicinal Chemistry. 2024; 67: 6705–6725. https://doi.org/10.1021/acs.jmedchem.4c00265

[17] Fan Y, Chen H, Mu N, Wang W, Zhu K, Ruan Z, et al. Nosiheptide analogues as potential antibacterial agents via dehydroalanine region modifications: Semi-synthesis, antimicrobial activity and molecular docking study. Bioorganic & Medicinal Chemistry. 2021; 31: 115970. https://doi.org/10.1016/j.bmc.2020.115970

[18] Yang J, Ling B, Chidambaram SB, Sakharkar MK. Pharmacokinetic study of two sulfamethoxazole-phytochemical antimicrobial conjugates in mice. Pharmazie. 2025; 80: 7–9. https://doi.org/10.1691/ph.2025.5510